Published in final edited form as:
Neuron. 2013 August 7; 79(3): 567–578. doi:10.1016/j.neuron.2013.06.008.

Motor cortex feedback influences sensory processing by modulating network state

Edward Zagha[1], **Amanda E. Casale**[1], **Robert N. S. Sachdev**[1], **Matthew J. McGinley**[1], and **David A. McCormick**[1,2]

[1]Department of Neurobiology, Yale School of Medicine, New Haven, Connecticut, USA

[2]Kavli Institute for Neuroscience, Yale School of Medicine, New Haven, Connecticut, USA

Summary

Long range cortico-cortical communication may have important roles in context-dependent sensory processing, yet we know very little about how these pathways influence their target regions. We studied the influence of primary motor cortex activity on primary somatosensory cortex in the mouse whisker system. We show that primary motor and somatosensory cortices undergo coherent, context-dependent changes in network state. Moreover, we show that motor cortex activity can drive changes in somatosensory cortex network state. A series of experiments demonstrate the involvement of the direct cortico-cortical feedback pathway, providing temporally precise and spatially targeted modulation of network dynamics. Cortically-mediated changes in network state significantly impact sensory coding, with activated states increasing the reliability of responses to complex stimuli. By influencing network state, cortico-cortical communication from motor cortex may ensure that during active exploration the relevant sensory region is primed for enhanced sensory discrimination.

Introduction

A remarkable feature of sensory perception is the ability to evaluate external stimuli according to momentary demands. This context-dependence of sensory perception is reflected in cortical representations of sensory stimuli, which are modulated by behavioral and cognitive states (Gazzaley and Nobre, 2012; Moran and Desimone, 1985; Nicolelis and Fanselow, 2002; Niell and Stryker, 2010; Reynolds and Chelazzi, 2004). While multiple mechanisms likely contribute to context-dependent sensory processing, long range cortico-cortical pathways may be particularly important. A prominent feature of sensory cortex is the convergence of feedforward and cortico-cortical feedback pathways at each stage of sensory processing (Felleman and Van Essen, 1991). While some have hypothesized that feedback pathways provide important internal and contextual cues that influence sensory perception (Cauller and Kulics, 1991; Engel et al., 2001; Lamme and Roelfsema, 2000), we know very little about how feedback inputs influence their target regions.

In addition to sensory representations, the rhythmic fluctuations of cortical circuits also exhibit dramatic context-dependent changes. Whereas low frequency, high amplitude EEG/LFP fluctuations correlate with inattentiveness and immobility, low amplitude, high

Correspondence should be addressed to D.A.M. (david.mccormick@yale.edu).

frequency EEG/LFP fluctuations, particularly in the gamma band, correlate with arousal, attention and behavior (Berger, 1929; Buzsaki, 2006; Fries et al., 2001; Moruzzi and Magoun, 1949; Poulet and Petersen, 2008). Traditionally, neocortical state changes have been attributed to ascending neuromodulatory systems (Buzsaki et al., 1988; Dringenberg and Vanderwolf, 1997; Jones, 2003; Lee and Dan, 2012; Metherate et al., 1992; Steriade et al., 1993b). However, considering the relatively slow time course and spatially distributed targets of neuromodulatory systems, it is unclear whether these pathways have permissive or instructive roles in moment-to-moment changes of network states. A recent study demonstrated strong thalamic contributions to cortical state (Poulet et al., 2012), suggesting that glutamatergic inputs may also modulate network state. Cortico-cortical feedback projections are well-positioned to mediate rapid and specific changes in network dynamics, and yet direct evidence for their roles in modulating network states has not been reported. Moreover, it is unclear how network state influences sensory processing, with proposed mechanisms including gain control, increased precision in temporal coding, and modulation of neuronal correlations (Engel et al., 2001; Goard and Dan, 2009; Haider et al., 2007; Haider and McCormick, 2009; Harris and Thiele, 2011; Hasenstaub et al., 2007; Marguet and Harris, 2011).

In this study, we focus on the contributions of motor cortex activity to sensory processing in the mouse whisker system. One potentially important pathway for providing contextual signals in the whisker system is the cortico-cortical feedback projection from the vibrissal portion of primary motor cortex (vM1) to the vibrissal representation in primary somatosensory cortex (S1) (Miyashita et al., 1994; Porter and White, 1983; Veinante and Deschenes, 2003). As vM1 neuronal activity correlates with whisking and other task-related parameters (Carvell et al., 1996; Erlich et al., 2011; Friedman et al., 2012; Hill et al., 2011; Huber et al., 2012; Petreanu et al., 2012), this pathway has been hypothesized to distribute the motor plan throughout the cortical whisker system (Kleinfeld et al., 2006; Kleinfeld et al., 1999). Recent studies have characterized responses of S1 neurons to vM1 stimulation *in vitro* (Petreanu et al., 2009; Rocco and Brumberg, 2007) and *in vivo* (Lee et al., 2008), demonstrating an excitatory effect of vM1 inputs most prominently onto infragranular S1 neurons. It is not fully understood, however, how vM1 feedback activity modulates S1 network dynamics, or how these signals integrate with sensory inputs and contribute to sensory processing.

We demonstrate that motor cortex activity can dramatically influence network dynamics in S1, during both whisking and non-whisking conditions. This modulation of network dynamics is rapid, exhibits target specificity, and is mediated at least in part by the direct cortico-cortical feedback pathway. Furthermore, we demonstrate that altering the network state directly influences sensory responses, and can modulate network response reliability and discrimination. We describe a cortical mechanism that directly links motor cortex activity to changes in somatosensory cortex network state, and may enhance representation of sensory inputs during active exploration.

Results

Simultaneous network state fluctuations in vM1 and S1 in waking mice

We recorded network activity simultaneously from ipsilateral vM1 and S1 in waking mice which had been habituated to head fixation (n=9 mice; recordings in LV of vM1 and S1). As previously described in S1 recordings (Crochet and Petersen, 2006; Petersen et al., 2003), we found that network activity in vM1 and S1 was highly variable and correlated with behavioral state (Figure 1A,C and Supplemental Figure 1A). When the mice were not whisking we often observed prominent slow, rhythmic LFP fluctuations at low frequencies (3–5 Hz). These LFP signals were associated with bursts of multiunit spiking interspersed

with brief (50–250 msec) periods of little or no spiking (Figure 1A, bottom left). During whisking, vM1 and S1 transitioned to activated states, characterized by suppression of low frequency LFP fluctuations, enhanced LFP activity in the gamma band and tonic multiunit spiking (Figure 1A, bottom center) (comparing whisking to non-whisking: S1, 1–5 Hz power: 66+/−7% decrease, $p<0.001$; 30–50 Hz power: 58+/−16% increase, $p<0.01$; MUA: 83+/−24% increase, $p<0.01$; vM1, 1–5 Hz power: 51+/−7% decrease, $p<0.001$; 30–50 Hz power: 34+/7% increase, $p<0.001$, MUA: 68+/−27% increase, $p<0.05$). Interestingly, we also observed prolonged activated states which were not coincident with whisking or any other obvious behaviors (Figure 1A, bottom right). Across these network states, activity in S1 and vM1 appeared remarkably synchronous. We found that S1 and vM1 were highly coherent at low frequencies (coherence at 2 Hz: 0.59 +/− 0.02), with a small yet reliable phase offset consistent with vM1 leading S1 (phase difference at 2 Hz: 8.8 +/− 3.2 degrees, lag=12.2 ms) (Supplemental Figure 1E,F).

Suppression of vM1 in waking mice partially deactivates S1

To determine the contributions of vM1 activity to S1 network dynamics, we suppressed vM1 activity by focal injection of $GABA_A$ agonist muscimol (n=9). Muscimol application caused a near complete suppression of spiking in vM1 (98+/−1% reduction, $p<0.0001$), and reduced power of the vM1 LFP at all frequencies (Supplemental Figure 1B). In S1, vM1 suppression caused a slowing of network activity (Figure 1B, Supplemental Figure 1D), resulting in enhanced power in low frequencies and reduced power in gamma frequencies of the S1 LFP (1–5 Hz power: 78+/−25% increase, $p<0.05$; 30–50 Hz power: 35+/−10% decrease, $p<0.05$; n=9) (Figure 1D–E). Suppressing vM1 significantly reduced, but did not abolish, whisking in the waking animal (percentage of time whisking during the recording session, control: 15+/−2%, vM1 suppression: 8+/−1%, $p<0.05$). To control for this behavioral change, we compared S1 LFP activity separately during whisking and non-whisking periods. We found that vM1 suppression caused a marked slowing of S1 network activity for both whisking and non-whisking periods (whisking, 1–5 Hz power: 109+/−38% increase, $p<0.05$; 30–50 Hz power: 29+/−13% decrease, $p<0.05$; non-whisking, 1–5 Hz power: 70+/−24% increase, $p<0.05$; 30–50 Hz power: 31+/−11% decrease, $p<0.05$). vM1 suppression did not abolish whisking-related changes in S1 dynamics (Figure 1B,E and Supplemental Figure 1C), but significantly affected the range of network dynamics experienced across these transitions (Figure 1B,E). Furthermore, vM1 suppression significantly reduced coherence between vM1 and S1 at low frequencies and reversed the phase relationship between these two areas (Supplemental Figure 1G,H). These data demonstrate that not only are S1 and vM1 network states correlated, but that vM1 activity contributes to rapid S1 dynamics across a variety of behavioral conditions.

Optogenetic excitation of vM1 activates S1 in waking mice

As vM1 suppression resulted in a marked slowing of S1 network activity, we next sought to determine the effects of vM1 stimulation. Channelrhodopsin-2 (ChR2) was expressed in vM1 neurons, either by injecting AAV encoding ChR2 focally into vM1 or by driving Cre-dependent ChR2 expression from the EMX1 locus (EMX-Cre:ChR2). To tonically stimulate vM1 neurons, we delivered prolonged (1–5 seconds) ramps of light at the vM1 dural surface while recording network activity in S1 (Figure 2). In waking mice (n=8 mice total, n=6 AAV-mediated ChR2 expression, n=2 EMX-Cre:ChR2 mice, data combined), vM1 stimulation activated S1, causing a significant decrease in S1 delta power and increase in MUA (1–4 Hz power: 58+/−6% decrease, $p<0.05$; MUA: 21+/−8% increase, $p<0.05$; 30–50 Hz power: 31+/−29% increase, $p=0.4$).

In a subset of mice (n=6) EMG recordings from the contralateral whisker pad enabled us to monitor whisker movements (Figure 2A,B). We found that whisker activity was enhanced

with vM1 stimulation, compared to matched spontaneous periods (30+/−9% increase in EMG signals, $p<0.05$). To determine the relationships between vM1 stimulation, S1 activity and whisking, we parsed S1 responses into whisking and non-whisking trials based on whisker pad EMG signals (Figure 2C). vM1 stimulation caused similar decreases in delta power for whisking and non-whisking trials (non-whisking: 54+/−7% decrease, $p<0.05$ compared to spontaneous; whisking: 57+/−11% decrease, $p<0.05$; $p=0.5$ comparing whisking and non-whisking) (Figure 2D), suggesting that vM1 modulation of S1 activity can be dissociated from whisking. However, MUA was significantly larger in whisking than non-whisking trials (33+/−9% larger, $p<0.05$), suggesting the recruitment of additional S1 inputs during whisking.

vM1 rapidly and selectively activates S1 neurons through cortical feedback in anesthetized mice

To eliminate the contribution of behavioral changes to network state, we conducted stimulation experiments in anesthetized mice. These experiments utilized only focal AAV-mediated ChR2 expression to ensure selective stimulation of vM1 neurons as opposed to fibers of passage, and we confirmed that this approach did not produce retrograde expression of ChR2 in somata of S1 neurons (n=5 injected mice; Supplemental Figure 3A–C).

vM1 stimulation in anesthetized mice dramatically altered S1 network dynamics, abolishing the slow oscillation and activating S1 (n=43 mice) (Figure 3A,B). Varying the intensity of vM1 stimulation caused graded decreases in delta power of the S1 LFP and graded increases in both gamma band power and multiunit spiking (Figure 3C–E) (comparing control to largest vM1 stimulation: 1–4 Hz power, 60+/−6% reduction, $p<0.0001$; 30–50 Hz power, 94+/−22% increase, $p<0.001$; MUA, 235+/−52% increase, $p<0.001$; n=9). These measurements of network activity had different sensitivities to vM1 stimulation, with delta power being most sensitive, followed by MUA and then gamma power (Supplemental Figure 2C,D). Furthermore, vM1-evoked modulation of S1 activity was very rapid, with S1 activity tightly following the time course of vM1 stimulation (Supplemental Figure 2E–G). At vM1 offset, S1 activity returned to slow oscillatory dynamics within tens of milliseconds (50% decay of S1 MUA: 16.3+/−2.9 ms, n=8) (Supplemental Figure 2F). These temporal characteristics differ considerably from stimulation of neuromodulatory systems, which produce cortical modulations at long latency and can persist for seconds after stimulus offset (Goard and Dan, 2009; Metherate et al., 1992). Laminar array recordings (n=6) demonstrated that vM1 stimulation eliminated slow oscillations in all cortical layers (data not shown) and increased spiking most prominently in infragranular neurons (as quantified by absolute increases in spike rate [Figure 3F] as well as percentage increases from baseline firing rates).

Whole cell recordings in vivo revealed that vM1 stimulation produced a sustained depolarization and high frequency membrane potential fluctuations in S1 neurons consistent with a depolarizing barrage of synaptic inputs (n=6) (Figure 3G,H). Similar to the S1 LFP, prolonged vM1 stimulation altered the frequency components of the membrane potential of S1 neurons, causing a decrease in delta power and increase in gamma band power (1–4 Hz power, 66+/−9% reduction, $p<0.05$; 30–50 Hz power, 78+/−18% increase, $p<0.01$). Furthermore, vM1 stimulation abolished the bimodal membrane potential distribution characteristic of anesthetized states (Steriade et al., 1993c), resulting in a membrane potential distribution similar to the Up state of the slow oscillation (Figure 3I,J) (n=6). Together, these data demonstrate that vM1 activity can robustly modulate S1 network dynamics, with exquisite control of timing and magnitude.

We next conducted a series of experiments to determine the pathways involved in vM1 modulation of S1 network activity. The network changes in S1 evoked by vM1 stimulation could be specific to the whisker system, or could reflect a global state change throughout the brain. To distinguish between these possibilities, we recorded simultaneously from S1 and V1 while stimulating vM1 (n=8). Overall, we found that activity in V1 was much less sensitive to vM1 stimulation than S1 (Figure 4). While vM1 stimulation caused significant increases in S1 gamma band power and MUA, we observed no significant changes of these measurements in simultaneous V1 recordings (Figure 4C,D) (30–50 Hz power: 47+/−12% increase in S1, 5+/−3% increase in V1, $p<0.01$ comparing S1 and V1 responses; MUA: 175+/−29% increase in S1, -4+/−15% increase in V1, $p<0.001$). Reductions in delta power of the LFP were consistently larger in S1 than V1 (Figure 4B) (58+/−7% reduction in S1, 35+/−12% reduction in V1, $p<0.05$), although we did observe a significant decrease in V1 delta power during vM1 stimulation ($p<0.05$). These results suggest that effects of vM1 stimulation are spatially targeted, at least at the resolution of these different sensory cortices.

To better characterize the vM1-evoked S1 input pathway, we determined the laminar profile of S1 responses. Specifically, we compared current-source density (CSD) patterns from multi-electrode array recordings in S1 in response to brief whisker deflection (n=5) or brief (5 ms) vM1 stimulation (n=8). As previously observed (Di et al., 1990), whisker deflection evoked current sinks in intermediate layers (Figure 5A). vM1 stimulation produced a markedly different response pattern, evoking current sinks in layers I and V/VI (Figure 5B). This CSD pattern is remarkably similar to the anatomical and functional targets of vM1-S1 cortico-cortical axons (Petreanu et al., 2009; Veinante and Deschenes, 2003) (Supplemental Figure 3A–C), suggesting that a significant portion of vM1-evoked effects may be mediated through the direct cortical pathway.

To test the efficacy of the cortico-cortical pathway, we stimulated vM1 axons in S1 and recorded S1 responses *in vitro* and *in vivo*. In acute slice preparations, we found remarkably high response rates to brief (2 ms) light pulses for both regular spiking and fast spiking neurons in layer V (Figure 5C,D) (80% of RS cells [12/15] and 44% of FS cells [4/9]), which likely represent lower bounds of connectivity in the intact brain. Moreover, response amplitudes ranged between 2.5 and 20 mV, suggesting that each S1 neuron receives multiple direct synaptic contacts from vM1. Second, we tested whether we could elicit S1 activation *in vivo* by directly stimulating cortico-cortical vM1 axons in S1 (1–5 second stimulus duration; n=3 continuous ramp illumination, n=1 high frequency repetitive illumination). Indeed, light stimulation of vM1 axons also activated S1 (Figure 5E) (delta power: 54+/−12% decrease, $p<0.05$; MUA: 77+/−11% increase, $p<0.01$; gamma power: 5+/−16% increase, $p=0.9$; consistent with moderate activation). In additional experiments (n=3), we applied muscimol focally in vM1 to limit network effects mediated by antidromic signaling. Under these conditions, light stimulation of vM1 axons was also effective at driving S1 spiking ($p<0.05$). These data support a mechanism of local S1 activation via direct and dense cortico-cortical projections from vM1 to S1.

While feedback projections to layer I are widely appreciated (Cauller, 1995; Larkum and Zhu, 2002; Petreanu et al., 2012), axons from vM1 ramify in layer I and infragranular layers (Petreanu et al., 2009; Veinante and Deschenes, 2003) (Supplemental Figure 3A–C). To investigate the contributions of this bilayer input to S1 activation, we applied AMPA/kainate receptor antagonist CNQX to the S1 pial surface to block rapid vM1 glutamatergic transmission (n=4) (Rocco and Brumberg, 2007). We used moderate concentrations of CNQX (100 μM) to suppress glutamatergic signaling in superficial layers and high concentrations (1 mM) to suppress signaling in all layers (see Supplemental Figure 3D–G for validation of this pharmacological strategy). We found that vM1-evoked MUA responses in layer II/III were highly sensitive to both concentrations of CNQX, whereas MUA

responses in layer V were significantly reduced by only high CNQX concentrations (Supplemental Figure 3H). These experiments suggest that the bilayer input from vM1 may preferentially drive spiking in different populations of S1 neurons and that deep layer inputs are sufficient for activation of infragranular S1 neurons.

vM1 activation of S1 occurs in the absence of thalamic input in anesthetized mice

Considering the numerous projections from vM1 to thalamic and other sub-cortical nuclei (Sharp and Evans, 1982), and recent work demonstrating powerful influences of thalamic pathways on S1 network states (Poulet et al., 2012), we next tested whether vM1 modulation of S1 activity requires thalamocortical transmission. For these experiments, we suppressed thalamic activity by focal muscimol injection targeted to the VPM, and measured S1 responses to vM1 stimulation. VPM suppression was validated by near complete elimination of whisker-evoked responses in S1 (n=9; data not shown).

Thalamic suppression had a substantial impact on ipsilateral S1 spontaneous activity. On multiunit spiking, thalamic suppression resulted in a prolongation of the Down state to greater than 1 second, with Up state activity appearing as brief bursts of action potentials (Figure 6D, Supplemental Figure 4B). Intracellular recordings showed that the prolonged periods of silence were associated with membrane hyperpolarization and marked absence of synaptic activity, while the action potential bursts were mediated by punctate depolarizations consistent with the arrival of strong barrages of synaptic potentials (Figure 6A). Accordingly, thalamic suppression affected multiple measurements of spontaneous S1 network activity (Up state frequency: 45+/−7% reduction; $p<0.01$; 1–4 Hz power: 32+/−10% reduction, $p<0.05$; 30–50 Hz power: 44+/−11% reduction, $p<0.05$; multiunit spike rate: 45+/−15% reduction, $p<0.05$; n=10) (Supplemental Figure 4E–G).

Despite changes in spontaneous activity, vM1 simulation robustly modulated S1 state during thalamic suppression (Figure 6). As observed from S1 whole cell recordings (n=5), vM1 stimulation caused sustained membrane potential depolarization (Figure 6A–C) and significantly increased membrane potential fluctuations in gamma band frequencies (30–50 Hz power, 194+/−59% increase, $p<0.05$). As in control conditions, vM1-mediated sustained depolarization exhibited features consistent with an ongoing and depolarizing barrage of synaptic activity (Figure 6A; n=5). vM1 stimulation during thalamic suppression evoked tonic S1 multiunit spiking (Figure 6E,G) and increased LFP power in the gamma band (Supplemental Figure 4C–G) (MUA: 22+/−16 fold increase, $p<0.05$; 30–50 Hz power: 239+/−54% increase, $p<0.05$) (n=7), consistent with the tonic depolarization observed from intracellular recordings (Figure 6A). Activation of S1 by vM1 stimulation also altered the relationship between action potential activity and the LFP, in both normal animals and following thalamic suppression. As observed in the spike-triggered average of the local field potential (STA-LFP), vM1 stimulation disrupted the phase-locking of spikes to the negative trough of the slow oscillation (Figure 6F–I). Consequently, there was a suppression of the delta power present in the STA-LFP with vM1 stimulation in both control conditions (STA-LFP delta power: 86+/−3% reduction, $p<0.0001$) and following thalamic suppression (75+/−8% reduction, $p<0.05$). Thus, while thalamocortical interactions strongly influence S1 network activity, cortico-cortical signaling can modulate S1 dynamics independent of the thalamus.

Modulation of vM1 activity alters sensory evoked responses in S1 in waking and anesthetized mice

Considering the ability of vM1 activity to modulate S1 state, we next asked how this modulation may impact sensory processing. In waking mice we recorded S1 responses to discrete whisker stimuli before (control) and during muscimol suppression of vM1 (n=6). In

control conditions, whisker stimuli evoked mono-phasic MUA and LFP responses (Figure 7A,C). In contrast, during vM1 suppression the same stimuli evoked bi-phasic MUA and LFP responses (Figure 7B,C). These latter signals consisted of onset increases in spiking, followed by prolonged spike suppression and positive-going LFP rebound potentials lasting hundreds of milliseconds. Consequently, S1 LFP delta power throughout the response period was enhanced 272+/−61% during vM1 suppression ($p<0.05$) (Figure 7D). We conducted a complementary set of experiments in anesthetized mice, briefly deflecting the principal whisker with or without pairing to vM1 stimulation (n=7). In control conditions, single sensory stimuli evoked long lasting rebound responses (Figure 7E), similar to vM1 suppression conditions in waking mice. Pairing of vM1 stimulation with sensory stimuli abolished the rebound responses, resulting in a 66+/−5% reduction in S1 LFP delta power during the response period ($p<0.001$) (Figure 7F). Thus, vM1 modulation of S1 spontaneous activity was strongly reflected in sensory responses, with enhanced vM1 activity reducing biphasic, low frequency S1 sensory responses.

We reasoned that the temporal characteristics of sensory responses may significantly affect the ability to encode and discriminate complex stimuli. Specifically, we hypothesized that when S1 network activity is dominated by spontaneous bursts of action potential activity, underlying the low frequencies of the local field potential, it would be less capable of reliably representing diverse sensory patterns. To test this, we constructed a set of stimulus patterns consisting of 10 short duration whisker deflections of varying velocity at 10 Hz (see Methods; Figure 8A), and applied these stimuli to anesthetized mice to enable precise, repeated delivery in the absence of spontaneous whisking. Each pattern was delivered to the principal whisker with and without pairing to vM1 stimulation while recording S1 network responses (n=7).

As observed in Figure 8B, pairing vM1 stimulation with sensory stimuli highly constrained the S1 responses. To assess MUA variability, we re-ordered the multiunit responses to individual stimuli across all patterns (Figure 8A,C) and quantified the MUA coefficient of variation (CV) (Figure 8D). Overall, vM1 stimulation caused a 32+/−4% reduction in CV across all stimuli ($p<0.001$) (Figure 8E). Notably, vM1 effects on variability were most pronounced for weaker stimuli, which normally produced the largest variability (Figure 8D, Supplemental Figure 5C,D). We also quantified the variability of single-trial LFP responses to the stimulus patterns. For each pattern, we calculated both the mean standard deviation of the LFP waveforms across time and the average cross-correlation from all pair-wise combinations of individual trials. Both approaches revealed reduced variability with vM1 stimulation (32+/−3% reduction in mean standard deviation, $p<0.001$; 60+/−26% increase in pair-wise cross-correlation, $p<0.01$) (Figure 8F).

Considering the reduction in S1 response variability with vM1 stimulation, we next assessed whether vM1 stimulation may enhance sensory response discrimination. We implemented a linear discriminant analysis (see Methods) to determine the ability to correctly classify single-trial responses amongst each of the eight whisker stimulus patterns. Indeed, we found that vM1 stimulation caused a significant increase in correct classification of both MUA and LFP responses (MUA: 22+/−12% increase, $p<0.05$; LFP: 24+/−12% increase, $p<0.05$; n=7) (Figure 8G).

As vM1 stimulation has a major impact on the frequency distribution of S1 activity, we wanted to determine whether different frequency components varied in their representation of sensory stimuli. We therefore filtered the single trial LFP responses into traditional frequency bands and applied the above analyses to the time-domain filtered signals. We observed steep frequency dependencies for both response variability and correction classification (Supplemental Figure 5E,F). For control and vM1 stimulation conditions, low

frequency signals were highly variable and poorly classified while signals in low gamma (30–50 Hz) were highly reliable with near optimal classification. Correlation and classification rates within frequency bands were similar for control and vM1 paired responses. However, vM1 stimulation dramatically shifted the frequency composition of the broadband LFP, causing a suppression of low frequency signals and enhancement of high frequency signals compared to control trials (Supplemental Figure 5G). Thus, improvements in variability and classification of S1 responses with vM1 stimulation are likely due to a reconfiguration of network dynamics, to minimize signals (e.g. slow rhythm) that poorly encode stimulus features and increase signals (e.g. 30–50 Hz activity) capable of enhanced sensory representation. Together, these data suggest that by modulating S1 network state, vM1 inputs to S1 may significantly affect sensory coding, including response variability and discrimination.

Discussion

We find that vM1 activity modulates S1 network states. Suppressing vM1 activity in waking mice causes a slowing of S1 dynamics during both whisking and non-whisking (Figure 1), and vM1 stimulation causes S1 activation in both waking and anesthetized mice (Figures 2 and 3). Multiple lines of evidence suggest the involvement of direct cortico-cortical projections from vM1 to S1 in modulating S1 state, including: the dense synaptic targeting of the cortico-cortical pathway, the block of S1 activation by glutamatergic receptor blocker CNQX, the contrasting CSD patterns evoked by vM1 versus sensory stimulation, the ability to activate S1 by directly stimulating vM1 axons in S1 and the ability of vM1 to modulate S1 activity during thalamic suppression.

Diverse mechanisms of neocortical network state modulation

Network state changes associated with arousal, attention and behavior have been largely ascribed to functions of ascending neuromodulatory systems (Buzsaki et al., 1988; Constantinople and Bruno, 2011; Jones, 2003; Lee and Dan, 2012; Steriade et al., 1993b). While cortico-cortical modulation of network state shares many similarities with neuromodulatory systems, there are notable differences. First, vM1-evoked S1 activation occurred with rapid temporal precision, tightly following the dynamics of the vM1 stimulus. In contrast, stimulation of neuromodulatory nuclei typically cause delayed changes in cortical dynamics that long outlast the stimulus (Goard and Dan, 2009; Metherate et al., 1992; Steriade et al., 1993a). Second, changes in vM1 stimulus strength caused graded changes in the LFP and MUA during the stimulus. Alternatively, varying stimulation intensity of ascending neuromodulatory inputs significantly impacts the duration of cortical activation (Metherate et al., 1992). While these differences in part could be due to optogenetic versus electrical stimulation methods, they likely reflect the time course of post-synaptic responses to ionotropic glutamate receptor activation versus metabotropic cholinergic or monoaminergic neurotransmission (McCormick et al., 1993). Third, we show that vM1-mediated network changes are spatially specific, consistent with the anatomy of cortico-cortical projections. In addition to cortical feedback, ascending thalamocortical pathways strongly regulate cortical state (Poulet et al., 2012) (Figure 6). Thus, we propose that not only neuromodulatory, but also glutamatergic feedforward and feedback pathways influence cortical states in the behaving animal. The anatomical and functional differences of these pathways allow for control of network states across a range of temporal and spatial scales that could be differentially employed according to momentary demands.

Motor cortex modulation of somatosensory network state, movement and non-movement contexts

Information processing in motor cortex may be rapidly relayed to the relevant sensory cortex via the direct feedback connection. One condition under which this may be important is during active movement. In the rodent whisker system, vM1 neuronal activity correlates with the initiation and envelope of whisking, with vM1 activity increasing prior to whisking onset [(Carvell et al., 1996; Friedman et al., 2012; Huber et al., 2012), but see (Hill et al., 2011)]. Importantly, a recent study specifically measured activity in S1-targeting vM1 feedback axons during a spatial discrimination task, and showed that this pathway increases its activity during whisking and other task parameters (Petreanu et al., 2012). Combined with our simultaneous recording, suppression and stimulation experiments, these data support a role for vM1 feedback in modulating S1 state during whisking. However, this is clearly not the only path for S1 modulation. During ipsilateral vM1 suppression we still observed robust changes in S1 with whisking (Supplemental Figure 1C), yet these transitions did not attain the normal levels of activation under control conditions (Figure 1E). Thus, multiple pathways converging onto S1 modulate network state during whisking, including signals relayed through thalamus (Poulet et al., 2012).

Motor cortex modulation of sensory cortex network state may also be important in the absence of overt movement. As in primate motor cortex (Churchland et al., 2010; Tanji and Evarts, 1976), rodent vM1 is involved in high-level motor planning (Brecht, 2011; Erlich et al., 2011). We found that vM1 stimulation can evoke S1 activation without evoking whisking (Figure 2), indicating a dissociation between cortical feedback and movement initiation. Furthermore, we found that vM1 suppression caused a slowing of S1 activity during quiet wakefulness, in addition to during whisking. Thus, vM1 may be a dynamic modulator of S1 state during movement and non-movement conditions. Future studies in mice engaging sensorimotor tasks are necessary to determine the range of conditions for which vM1 modulation of S1 state may contribute to sensory processing.

Role of network state in context-dependent sensory processing

Previous studies in the whisker system have shown that behavior strongly influences sensory responses. In general, during quiet wakefulness sensory responses are larger in amplitude and lateral spread within cortex compared to during whisking (Crochet and Petersen, 2006; Fanselow and Nicolelis, 1999; Ferezou et al., 2007; Hentschke et al., 2006; Krupa et al., 2004). These different cortical representations of the same sensory stimuli suggest that S1 may operate in different sensory processing modes depending on behavior. Specifically, the large and spatially extended responses during quiet wakefulness may reflect an optimization for object detection, whereas the reduced amplitude and lateral cortical spread of sensory responses during whisking may better enable feature or spatial discrimination (Nicolelis and Fanselow, 2002).

Our data extend these findings by emphasizing the importance of network state on somatosensory processing mode. We find that vM1 activity changes S1 sensory response dynamics (Figure 7), likely due to elimination of the intrinsic slow, rhythmic activity of the underlying network. Furthermore, we find that optimal sensory coding of complex stimuli is highly frequency-dependent, with enhanced trial-to-trial correlation and improved discrimination of the higher frequency components of sensory response signals (Supplemental Figure 5E,F). As cortical activation reconfigures network dynamics towards higher frequency components, we propose that network state is a major determinant of somatosensory processing mode. However, other mechanisms likely contribute to changes in sensory responses with vM1 modulation, including vM1-mediated suppression of

brainstem sensory responses and S1-VPM corticothalamic modulation of thalamic response properties (Lee et al., 2008; McCormick and von Krosigk, 1992; Wolfart et al., 2005).

Convergent data strongly argue for the importance of network state in modulating cortical sensory representations, regardless of the initiating mechanism. Previous studies in visual and auditory cortices demonstrated that neuromodulatory-evoked activation improves cortical representations of rapidly changing sensory inputs (Goard and Dan, 2009; Marguet and Harris, 2011). Similarly, spontaneous network state transitions from inactive to active during the slow oscillation also impact sensory coding; whereas S1 responses to brief whisker deflections are larger in the inactive Down state, coding of complex stimuli is enhanced during the active period represented by the Up state (Hasenstaub et al., 2007; Sachdev et al., 2004). Low frequency fluctuations of network activity in slow, rhythmic states are intrinsically generated and strongly contribute to sensory response variability (Arieli et al., 1996). Our data further support the hypothesis that activated states improve sensory representation in large part by minimizing intrinsic, low frequency fluctuations of network activity (Marguet and Harris, 2011). Furthermore, as modulation of sensory representation by network state has been shown in visual, auditory and somatosensory cortices, network state is undoubtedly a fundamental determinant of sensory processing.

Long-range cortico-cortical feedback pathways are poised to distribute contextual signals throughout sensory cortices, and we propose modulation of network state as a simple yet powerful mechanism by which these feedback pathways influence sensory processing. The speed and spatial specificity of glutamatergic feedback projections make them ideal candidates to rapidly affect sensory processing according to momentary contextual cues and behavioral demands. Further research is required to determine whether cortico-cortical activation occurs in other sensory modalities, by non-motor feedback pathways, and thus may be a general mechanism of context-dependent sensory processing.

Experimental Procedures

Animal preparation and surgery

All protocols are in accordance with Yale University Institutional Animal Care and Use Committee. For experiments in waking mice, a light-weight metal head-holder with recording well was chronically implanted onto the skull of 2–3 month old C57BL/6 wild type or EMX-Cre:ChR2 mice under ketamine (90 mg/kg, ip) and xylazine (10 mg/kg, ip) anesthesia. For EMG recordings, fine tungsten wires (A-M Systems) were threaded into the whisker pad. After 4–7 days of habituation to head fixation, craniotomies over vM1 and S1 (<0.5 mm in diameter) were established under isoflurane anesthesia using stereotactic coordinates (from bregma [in mm], vM1: 1 rostral, 1 lateral; S1: 1.5 caudal, 3.5 lateral). Recordings from waking mice commenced at least 1–2 hours after surgery, allowing recovery from anesthesia such that the animals appeared to be behaving normally in their own cages prior to head fixation. For recordings under anesthesia, 2–3 month old mice were sedated with chlorprothixene (5 mg/kg, ip) and anesthetized with urethane (0.7 g/kg, ip). The head-holder was adhered to the skull, and two or three craniotomies were established over vM1, S1 and V1 (from bregma [in mm], V1: 3.5 caudal, 2.25 lateral). For focal muscimol injections, a glass pipette containing 2 mM muscimol (Tocris) was lowered into vM1 or VPM (from bregma [in mm], VPM: 1.8 caudal, 1.5 lateral, 3 ventral) and slowly volume injected (0.5–0.7 μL over 10 min). Recordings were conducted 1–2 hours following muscimol injection.

Electrophysiological recordings

LFP/MUA signals were obtained with tungsten microelectrodes (0.3–1 MΩ resistance, FHC) or 16 channel multielectrode arrays (A16, 177 μm^2 site area, NeuroNexus). Single microelectrodes were targeted to layer V at depths ranging from 750–850 μm, whereas multielectrode arrays spanned the full cortical depth. Signals were processed through a preamplifier (Multichannel Systems) and amplifier (A-M Systems 3500), bandpass filtered between 0.3 and 5 kHz and digitized at 10 kHz (Power 1401, CED). 'Blind' whole cell recordings in vivo (Margrie et al., 2002) and IR-DIC guided whole cell recordings in vitro were targeted to layer V neurons. Standard patch pipettes (4–6 MΩ) were used containing (in mM): 130 K-gluconate, 7 KCl, 4 Mg-ATP, 10 Na-phosphocreatine, 0.3 Na-GTP, 10 Hepes, 0.2–0.4% biocytin, pH 7.3 with KOH. Signals were processed using an AxoClamp-2B or Multiclamp 700B (Axon Instruments), filtered at 10 kHz and digitized at 20–40 kHz.

Stimulus delivery and video monitoring

ChR2 was activated by an LED-based light source (460 nm, Prizmatix) and multimode optical fiber (0.37 NA, 300 μm diameter, 30 mW/mm^2 maximum intensity at fiber terminus for stimulation in vM1; 0.48 NA, 1 mm diameter, 120 mW/mm^2 maximum intensity for stimulation in S1 both in vivo and in vitro). The optical fiber was positioned at the meningeal surface above vM1 or S1 (in vivo) or approximately 1 mm above the brain slice (in vitro). Whereas continuous ramp illumination was used for vM1 stimulation, continuous or high frequency repetitive illumination was used for axonal stimulation in vivo. Ramps were used instead of square pulse stimuli to minimize onset transient responses. Prolonged vM1 stimulation under anesthesia neither evoked whisker movements nor disrupted the spontaneous slow rhythmic whisker twitching in lightly anesthetized mice. Moreover, there were no effects of vM1 light stimulation on S1 activity in wild type or sham infected animals (n=4) (Supplemental Figure 2B). We tested a range of vM1 stimulation intensities (Figure 3), and used 10–20 mW/mm^2 throughout the rest of the study. For in vitro recordings, responses were considered mono-synaptic if they initiated within 4 ms from the onset of the stimulus. Whisker stimulation in waking mice was performed by air puff (10 ms) in the caudal direction at the whisker row eliciting the largest LFP response. We delivered 6 successive stimuli at 3 Hz (Figure 7A,B), and analyzed the three terminal responses to isolate sensory from startle responses.

Whisker deflections in anesthetized mice were controlled by a glass pipette attached to a piezoelectric stimulator (Physik Instrumente), deflecting in the caudal direction. The principal whisker was identified as the whisker stimulus evoking the shortest latency response. Each deflection of the principal whisker consisted of a 5 ms ramp to varying maximum amplitude, with instantaneous offset. Within a given stimulus pattern the amplitudes varied uniformly from 0.7 to 7°, sampling a range of velocities from 140 to 1400 degrees per second. Each stimulus pattern contained all 10 velocities, and a set of 8 different patterns were created by random permutation. 10 Hz frequency was chosen to simulate the frequency of rhythmic whisking. During waking recordings, whisker movements were video recorded (Logitech) and manually scored or monitored by EMG recordings from the whisker pad. 'Spontaneous whisking' and 'quiet wakefulness' were selected solely based on behavior, as sustained periods (>2 s) of whisking or non-whisking, respectively.

Data analyses

Analyses were conducted in Matlab (The Mathworks). Multiunit spike times were determined as threshold crossings well isolated (> 2X amplitude) from background noise. LFP was isolated by lowpass filtering offline (100 Hz cutoff, 5^{th} order Bessel filter). LFP signals were further downsampled to 200 Hz for standard deviation and classification

analyses. Membrane potential recording data were median filtered with a 10 ms sliding window to truncate spikes. Power spectral density and coherence were calculated using a multitaper method with 2 tapers (Borisovska et al., 2011). Time-frequency analyses used a 1 second sliding window with 50% overlap. In waking mice, slow, rhythmic oscillations typically occurred at frequencies of up to 5 Hz, and therefore we calculated 'low frequencies' as 1–5 Hz (Figure 1). Similar results were obtained by analyzing delta frequencies (1–4 Hz), which was used throughout the rest of the study. CSD was calculated as the second spatial derivative. Signals from EMG wires were high-pass filtered (100 Hz) and rectified.

Coefficient of variation (CV) analysis was used to characterize MUA variability. MUA responses to each whisker stimulus pattern were sorted in order to align each stimulus velocity across all patterns (Figure 8A). MUA responses were segmented into spike histograms (20 ms bins). CV was calculated independently for each time bin and averaged across all stimuli. LFP variability was characterized from single trial responses to each stimulus pattern. We calculated both the average standard deviation throughout the response period, and the mean correlation coefficient from all possible pair-wise cross-correlation calculations. Linear discrimination with diagonal covariance matrix estimates was used for classification analyses. Separate data were used to train and test the classifier using the leave-one-out method (9 trials for training, 1 trial for testing, iterated 10 times per experiment). Separate classifiers were used for control and vM1 stimulation trials. For MUA classification, results using 20 ms binning are shown, although similar results were obtained for a range of spike histogram bin sizes. Frequency-dependent classification analyses used the time-domain filtered LFP signals, and we retrained the classifier for each frequency band data set. Data are presented as mean ± standard error, unless otherwise specified. Statistical testing was performed using Student's t test, paired or unpaired as appropriate, and one-way ANOVA or one-way repeated measures ANOVA, for individual and population data respectively.

Supplementary Material

Refer to Web version on PubMed Central for supplementary material.

Acknowledgments

We thank Matthew Krause and James Mazer for many helpful discussions. We thank Flavio Frohlich for guidance on multielectrode recordings and analysis and Peter O'Brien for technical guidance. We thank Babak Tahvildari and Renata Batista-Brito for comments on the manuscript. This work was supported by NIH NS026143, NS007224 and Kavli Institute for Neuroscience (DAM) and NIH F32NS077816 (EZ).

References

Arieli A, Sterkin A, Grinvald A, Aertsen A. Dynamics of ongoing activity: explanation of the large variability in evoked cortical responses. Science. 1996; 273:1868–1871. [PubMed: 8791593]

Berger H. Ueber das Elektroenkephalogramm des Menschen. Arch Psychiatr Nervenkrankh. 1929; 87:527–570.

Borisovska M, McGinley MJ, Bensen A, Westbrook GL. Loss of olfactory cell adhesion molecule reduces the synchrony of mitral cell activity in olfactory glomeruli. J Physiol. 2011; 589:1927–1941. [PubMed: 21486802]

Brecht M. Movement, confusion, and orienting in frontal cortices. Neuron. 2011; 72:193–196. [PubMed: 22017982]

Buzsaki, G. Rhythms of the brain. New York: Oxford University Press; 2006.

Buzsaki G, Bickford RG, Ponomareff G, Thal LJ, Mandel R, Gage FH. Nucleus basalis and thalamic control of neocortical activity in the freely moving rat. J Neurosci. 1988; 8:4007–4026. [PubMed: 3183710]

Carvell GE, Miller SA, Simons DJ. The relationship of vibrissal motor cortex unit activity to whisking in the awake rat. Somatosens Mot Res. 1996; 13:115–127. [PubMed: 8844960]

Cauller L. Layer I of primary sensory neocortex: where top-down converges upon bottom-up. Behav Brain Res. 1995; 71:163–170. [PubMed: 8747184]

Cauller LJ, Kulics AT. The neural basis of the behaviorally relevant N1 component of the somatosensory-evoked potential in SI cortex of awake monkeys: evidence that backward cortical projections signal conscious touch sensation. Exp Brain Res. 1991; 84:607–619. [PubMed: 1864331]

Churchland MM, Cunningham JP, Kaufman MT, Ryu SI, Shenoy KV. Cortical preparatory activity: representation of movement or first cog in a dynamical machine? Neuron. 2010; 68:387–400. [PubMed: 21040842]

Constantinople CM, Bruno RM. Effects and mechanisms of wakefulness on local cortical networks. Neuron. 2011; 69:1061–1068. [PubMed: 21435553]

Crochet S, Petersen CC. Correlating whisker behavior with membrane potential in barrel cortex of awake mice. Nat Neurosci. 2006; 9:608–610. [PubMed: 16617340]

Di S, Baumgartner C, Barth DS. Laminar analysis of extracellular field potentials in rat vibrissa/barrel cortex. J Neurophysiol. 1990; 63:832–840. [PubMed: 2341880]

Dringenberg HC, Vanderwolf CH. Neocortical activation: modulation by multiple pathways acting on central cholinergic and serotonergic systems. Exp Brain Res. 1997; 116:160–174. [PubMed: 9305825]

Engel AK, Fries P, Singer W. Dynamic predictions: oscillations and synchrony in top-down processing. Nat Rev Neurosci. 2001; 2:704–716. [PubMed: 11584308]

Erlich JC, Bialek M, Brody CD. A cortical substrate for memory-guided orienting in the rat. Neuron. 2011; 72:330–343. [PubMed: 22017991]

Fanselow EE, Nicolelis MA. Behavioral modulation of tactile responses in the rat somatosensory system. J Neurosci. 1999; 19:7603–7616. [PubMed: 10460266]

Felleman DJ, Van Essen DC. Distributed hierarchical processing in the primate cerebral cortex. Cereb Cortex. 1991; 1:1–47. [PubMed: 1822724]

Ferezou I, Haiss F, Gentet LJ, Aronoff R, Weber B, Petersen CC. Spatiotemporal dynamics of cortical sensorimotor integration in behaving mice. Neuron. 2007; 56:907–923. [PubMed: 18054865]

Friedman WA, Zeigler HP, Keller A. Vibrissae motor cortex unit activity during whisking. J Neurophysiol. 2012; 107:551–563. [PubMed: 21994257]

Fries P, Reynolds JH, Rorie AE, Desimone R. Modulation of oscillatory neuronal synchronization by selective visual attention. Science. 2001; 291:1560–1563. [PubMed: 11222864]

Gazzaley A, Nobre AC. Top-down modulation: bridging selective attention and working memory. Trends Cogn Sci. 2012; 16:129–135. [PubMed: 22209601]

Goard M, Dan Y. Basal forebrain activation enhances cortical coding of natural scenes. Nat Neurosci. 2009; 12:1444–1449. [PubMed: 19801988]

Haider B, Duque A, Hasenstaub AR, Yu Y, McCormick DA. Enhancement of visual responsiveness by spontaneous local network activity in vivo. J Neurophysiol. 2007; 97:4186–4202. [PubMed: 17409168]

Haider B, McCormick DA. Rapid neocortical dynamics: cellular and network mechanisms. Neuron. 2009; 62:171–189. [PubMed: 19409263]

Harris KD, Thiele A. Cortical state and attention. Nat Rev Neurosci. 2011; 12:509–523. [PubMed: 21829219]

Hasenstaub A, Sachdev RN, McCormick DA. State changes rapidly modulate cortical neuronal responsiveness. J Neurosci. 2007; 27:9607–9622. [PubMed: 17804621]

Hentschke H, Haiss F, Schwarz C. Central signals rapidly switch tactile processing in rat barrel cortex during whisker movements. Cereb Cortex. 2006; 16:1142–1156. [PubMed: 16221924]

Hill DN, Curtis JC, Moore JD, Kleinfeld D. Primary motor cortex reports efferent control of vibrissa motion on multiple timescales. Neuron. 2011; 72:344–356. [PubMed: 22017992]

Huber D, Gutnisky DA, Peron S, O'Connor DH, Wiegert JS, Tian L, Oertner TG, Looger LL, Svoboda K. Multiple dynamic representations in the motor cortex during sensorimotor learning. Nature. 2012; 484:473–478. [PubMed: 22538608]

Jones BE. Arousal systems. Front Biosci. 2003; 8:s438–451. [PubMed: 12700104]

Kleinfeld D, Ahissar E, Diamond ME. Active sensation: insights from the rodent vibrissa sensorimotor system. Curr Opin Neurobiol. 2006; 16:435–444. [PubMed: 16837190]

Kleinfeld D, Berg RW, O'Connor SM. Anatomical loops and their electrical dynamics in relation to whisking by rat. Somatosens Mot Res. 1999; 16:69–88. [PubMed: 10449057]

Krupa DJ, Wiest MC, Shuler MG, Laubach M, Nicolelis MA. Layer-specific somatosensory cortical activation during active tactile discrimination. Science. 2004; 304:1989–1992. [PubMed: 15218154]

Lamme VA, Roelfsema PR. The distinct modes of vision offered by feedforward and recurrent processing. Trends Neurosci. 2000; 23:571–579. [PubMed: 11074267]

Larkum ME, Zhu JJ. Signaling of layer 1 and whisker-evoked Ca2+ and Na+ action potentials in distal and terminal dendrites of rat neocortical pyramidal neurons in vitro and in vivo. J Neurosci. 2002; 22:6991–7005. [PubMed: 12177197]

Lee S, Carvell GE, Simons DJ. Motor modulation of afferent somatosensory circuits. Nat Neurosci. 2008; 11:1430–1438. [PubMed: 19011625]

Lee SH, Dan Y. Neuromodulation of brain States. Neuron. 2012; 76:209–222. [PubMed: 23040816]

Margrie TW, Brecht M, Sakmann B. In vivo, low-resistance, whole-cell recordings from neurons in the anaesthetized and awake mammalian brain. Pflugers Arch. 2002; 444:491–498. [PubMed: 12136268]

Marguet SL, Harris KD. State-dependent representation of amplitude-modulated noise stimuli in rat auditory cortex. J Neurosci. 2011; 31:6414–6420. [PubMed: 21525282]

McCormick DA, von Krosigk M. Corticothalamic activation modulates thalamic firing through glutamate "metabotropic" receptors. Proc Natl Acad Sci U S A. 1992; 89:2774–2778. [PubMed: 1313567]

McCormick DA, Wang Z, Huguenard J. Neurotransmitter control of neocortical neuronal activity and excitability. Cereb Cortex. 1993; 3:387–398. [PubMed: 7903176]

Metherate R, Cox CL, Ashe JH. Cellular bases of neocortical activation: modulation of neural oscillations by the nucleus basalis and endogenous acetylcholine. J Neurosci. 1992; 12:4701–4711. [PubMed: 1361197]

Miyashita E, Keller A, Asanuma H. Input-output organization of the rat vibrissal motor cortex. Exp Brain Res. 1994; 99:223–232. [PubMed: 7523173]

Moran J, Desimone R. Selective attention gates visual processing in the extrastriate cortex. Science. 1985; 229:782–784. [PubMed: 4023713]

Moruzzi G, Magoun HW. Brain stem reticular formation and activation of the EEG. Electroencephalogr Clin Neurophysiol. 1949; 1:455–473. [PubMed: 18421835]

Nicolelis MA, Fanselow EE. Thalamocortical [correction of Thalamcortical] optimization of tactile processing according to behavioral state. Nat Neurosci. 2002; 5:517–523. [PubMed: 12037519]

Niell CM, Stryker MP. Modulation of visual responses by behavioral state in mouse visual cortex. Neuron. 2010; 65:472–479. [PubMed: 20188652]

Petersen CC, Hahn TT, Mehta M, Grinvald A, Sakmann B. Interaction of sensory responses with spontaneous depolarization in layer 2/3 barrel cortex. Proc Natl Acad Sci U S A. 2003; 100:13638–13643. [PubMed: 14595013]

Petreanu L, Gutnisky DA, Huber D, Xu NL, O'Connor DH, Tian L, Looger L, Svoboda K. Activity in motor-sensory projections reveals distributed coding in somatosensation. Nature. 2012; 489:299–303. [PubMed: 22922646]

Petreanu L, Mao T, Sternson SM, Svoboda K. The subcellular organization of neocortical excitatory connections. Nature. 2009; 457:1142–1145. [PubMed: 19151697]

Porter LL, White EL. Afferent and efferent pathways of the vibrissal region of primary motor cortex in the mouse. J Comp Neurol. 1983; 214:279–289. [PubMed: 6853758]

Poulet JF, Fernandez LM, Crochet S, Petersen CC. Thalamic control of cortical states. Nat Neurosci. 2012; 15:370–372. [PubMed: 22267163]

Poulet JF, Petersen CC. Internal brain state regulates membrane potential synchrony in barrel cortex of behaving mice. Nature. 2008; 454:881–885. [PubMed: 18633351]

Reynolds JH, Chelazzi L. Attentional modulation of visual processing. Annu Rev Neurosci. 2004; 27:611–647. [PubMed: 15217345]

Rocco MM, Brumberg JC. The sensorimotor slice. J Neurosci Methods. 2007; 162:139–147. [PubMed: 17307257]

Sachdev RN, Ebner FF, Wilson CJ. Effect of subthreshold up and down states on the whisker-evoked response in somatosensory cortex. J Neurophysiol. 2004; 92:3511–3521. [PubMed: 15254074]

Sharp FR, Evans K. Regional (14C) 2-deoxyglucose uptake during vibrissae movements evoked by rat motor cortex stimulation. J Comp Neurol. 1982; 208:255–287. [PubMed: 7119161]

Steriade M, Amzica F, Nunez A. Cholinergic and noradrenergic modulation of the slow (approximately 0.3 Hz) oscillation in neocortical cells. J Neurophysiol. 1993a; 70:1385–1400. [PubMed: 8283204]

Steriade M, McCormick DA, Sejnowski TJ. Thalamocortical oscillations in the sleeping and aroused brain. Science. 1993b; 262:679–685. [PubMed: 8235588]

Steriade M, Nunez A, Amzica F. A novel slow (< 1 Hz) oscillation of neocortical neurons in vivo: depolarizing and hyperpolarizing components. J Neurosci. 1993c; 13:3252–3265. [PubMed: 8340806]

Tanji J, Evarts EV. Anticipatory activity of motor cortex neurons in relation to direction of an intended movement. J Neurophysiol. 1976; 39:1062–1068. [PubMed: 824409]

Veinante P, Deschenes M. Single-cell study of motor cortex projections to the barrel field in rats. J Comp Neurol. 2003; 464:98–103. [PubMed: 12866130]

Wolfart J, Debay D, Le Masson G, Destexhe A, Bal T. Synaptic background activity controls spike transfer from thalamus to cortex. Nat Neurosci. 2005; 8:1760–1767. [PubMed: 16261132]

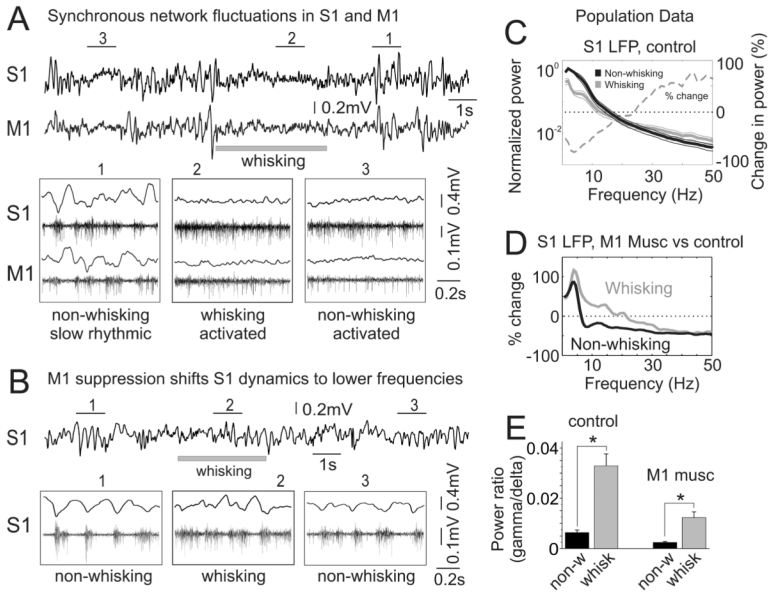

Figure 1. Suppressing vM1 in waking mice shifts S1 network dynamics to lower frequencies

(A) Top traces, simultaneous LFP recordings in S1 (top) and vM1 (bottom) in a head-fixed, waking mouse. A period of spontaneous whisking is noted by the gray bar. Bottom traces, expanded regions of above, showing LFP (top) and MUA (bottom) for both S1 and vM1 recordings. Note activated network dynamics in S1 and vM1 associated with both whisking and non-whisking periods, and slow rhythmic dynamics during non-whisking. (B) Layout as above, recording from the same S1 site during focal vM1 suppression by local muscimol injection. LFP and MUA display enhanced slow rhythmic features, during both whisking and non-whisking. (C–E) Population data, analyses of S1 LFP signals, parsed into whisking (gray) and non-whisking (black) periods. (C) Normalized S1 LFP power spectra during control conditions, comparing whisking and non-whisking; thick lines are mean, thin lines +/− standard error. The gray dashed line is percent change [100*(whisking-non)/non], referencing scales at the right border of the graph. Dotted black lines [C,D] indicate zero change in power. (D) Changes in the S1 LFP power spectra comparing control and vM1 muscimol conditions [100*(muscimol-control)/control], for whisking and non-whisking periods. Positive-going changes indicate increased power during vM1 suppression. (E) Comparisons of S1 LFP gamma/delta power ratio for control (left) and vM1 muscimol (right) conditions. In both conditions whisking increased the gamma/delta ratio, although vM1 suppression significantly impacted the range of modulation. Bar graphs (in all figures) are mean +/− standard error. *, $p<0.01$. See also Supplemental Figure 1.

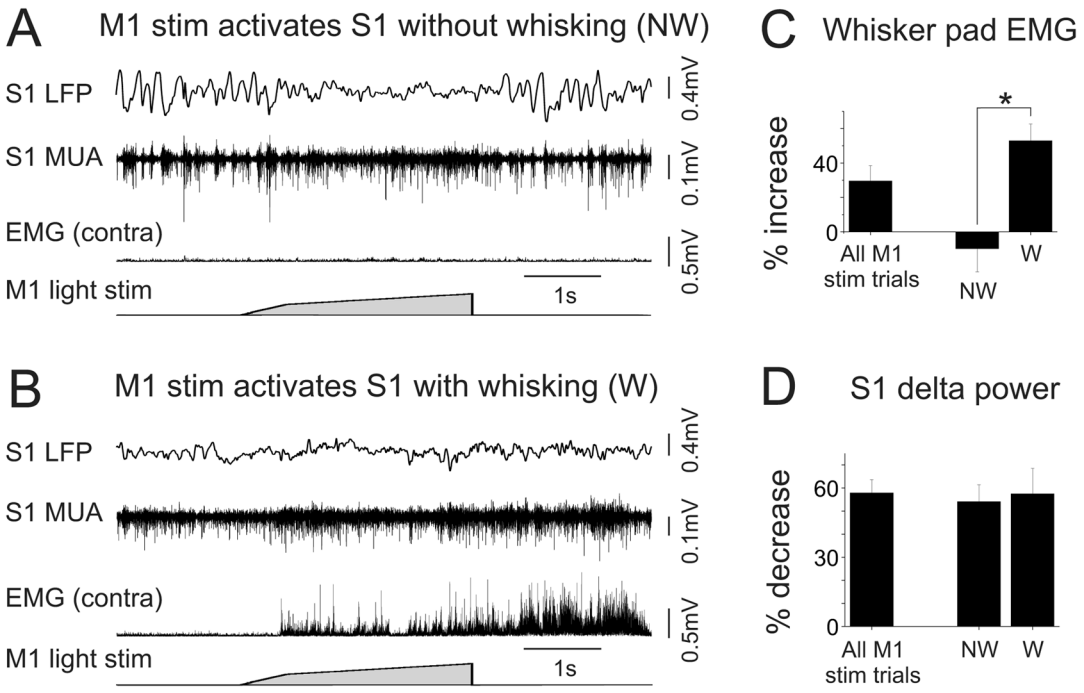

Figure 2. vM1 stimulation in waking mice modulates whisking activity and S1 state

(A,B) LFP and MUA recordings from layer V of S1 in a head-fixed waking mouse while monitoring contralateral whisker pad EMG activity and delivering vM1 stimuli. (A) An example of vM1-evoked S1 activation in the absence of whisking. Note the return of slow, rhythmic network activity following stimulus offset. (B) An example of vM1-evoked S1 activation associated with whisking. In this trial whisking outlasted the vM1 stimulus, and the network remained activated throughout the whisking period. (C) Population data of whisker pad EMG signals during vM1 stimulation compared to spontaneous periods. The right bars depict the results from sorting vM1 responses into whisking (W) and non-whisking (NW) trials. (D) Population data of decreases in S1 LFP delta power during vM1 stimulation compared to spontaneous periods. vM1 stimulation caused similar decreases in S1 delta power in whisking and non-whisker trials. *, $p<0.05$.

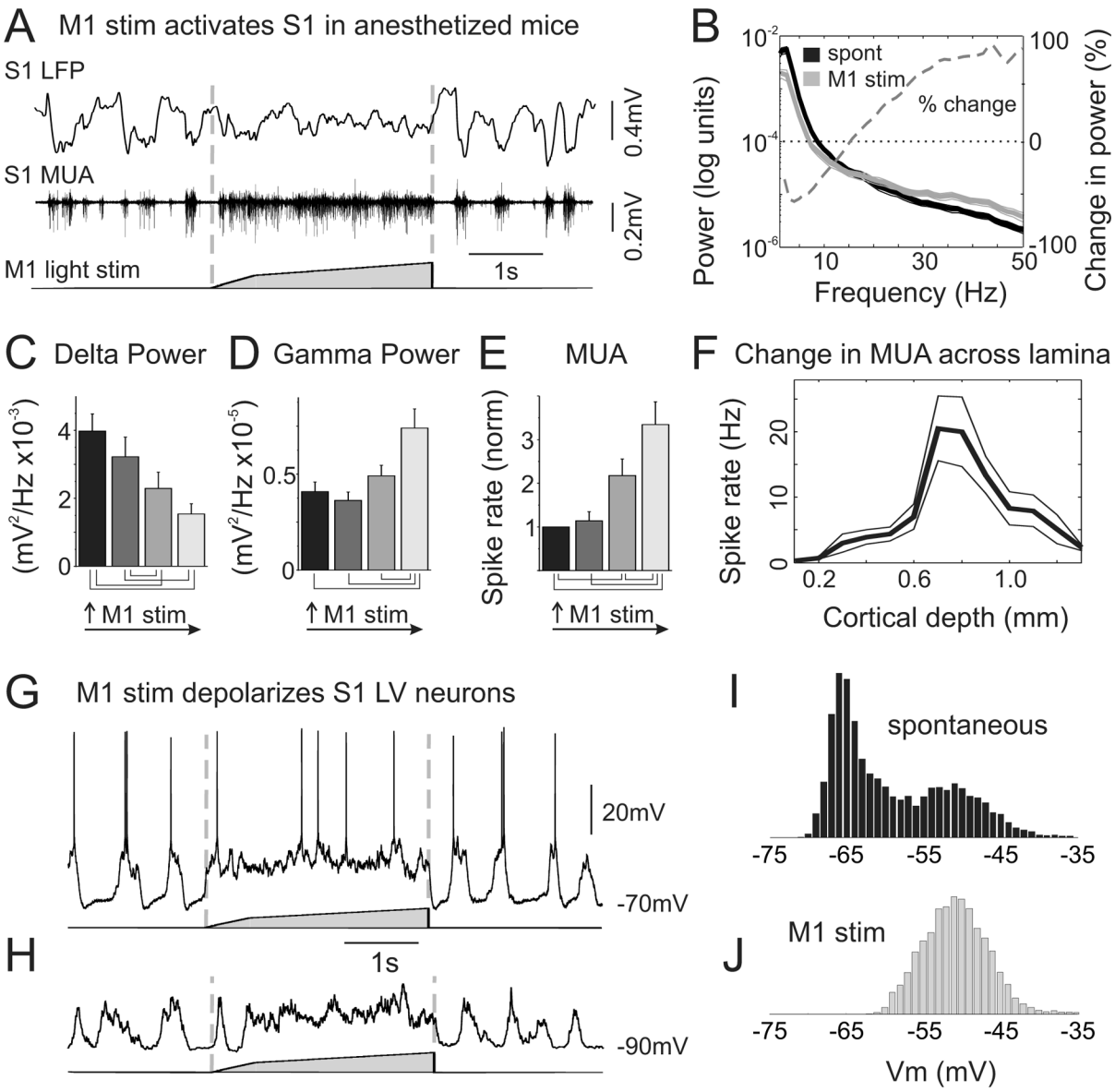

Figure 3. vM1 stimulation in anesthetized mice activates S1

(A) Example recording from LV of S1, showing LFP (top) and MUA (middle) in response to a three second vM1 light stimulus (bottom). Note that the slow oscillations, present immediately before and after the stimulus, are disrupted throughout the vM1 stimulation. (B) Population average power spectra from S1 recordings of spontaneous activity (black) and during vM1 stimulation (gray). Gray dashed line is the percent change in power [100*(stim-spont)/spont] demonstrating reduced power at delta frequencies and increased power at gamma frequencies with vM1 stimulation. Dotted black line indicates zero power change. (C–E) Population data, comparing spontaneous S1 activity (black) to responses from increasing intensities of vM1 light stimulation. Note graded changes in delta power (C), gamma power (D) and MUA (E). Lines below bar graphs denote differences of statistical significance from Tukey post-hoc pairwise comparisons, $p<0.05$. (F) Population data from laminar multielectrode recordings, showing S1 spike rate increases across all layers during S1 activation. Spontaneous spike rates have been subtracted to isolate vM1-evoked activity. (G) A whole cell current clamp recording from a layer V S1 neuron, in

response to a three second vM1 stimulus. vM1 stimulation produced a sustained depolarization with high frequency membrane potential fluctuations. (H) Same recording as above, hyperpolarized by DC to eliminate spiking. (I,J) Vm histograms of the neuron shown in [G], during spontaneous periods (I) and during vM1 stimulation (J). See also Supplemental Figure 2.

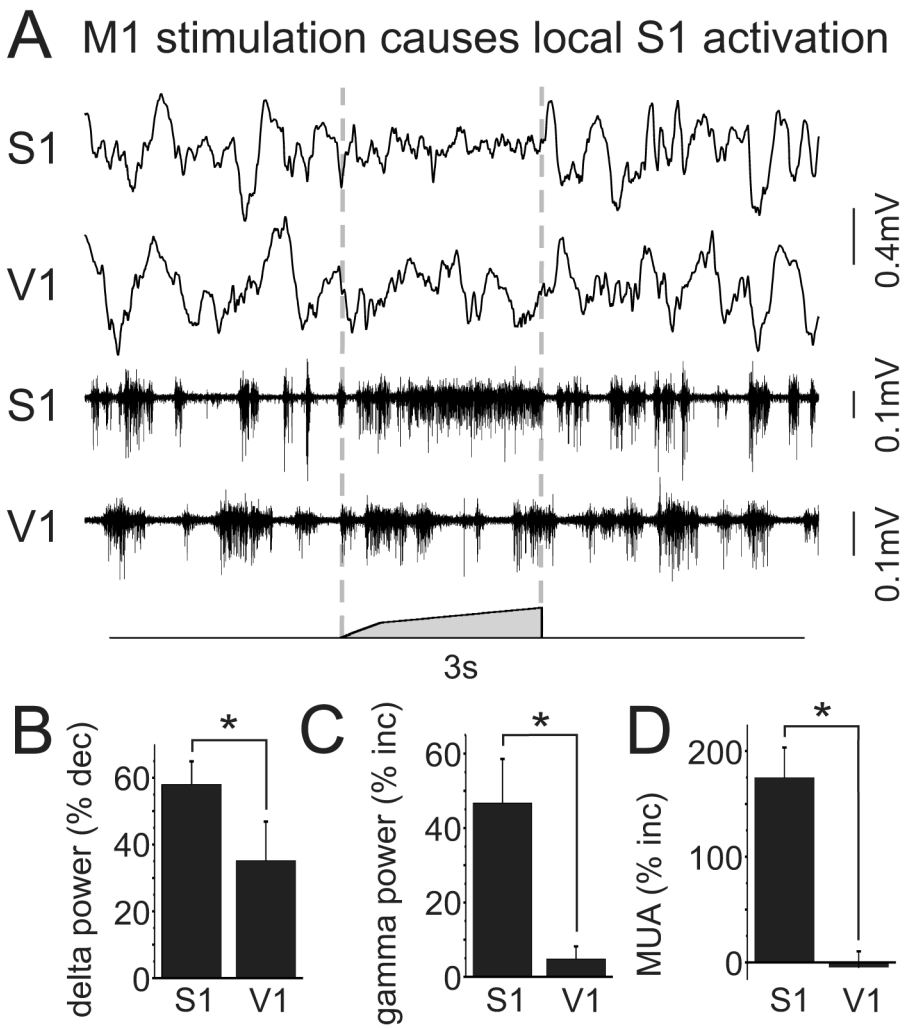

Figure 4. vM1 stimulation causes local S1 activation

(A) Simultaneous recordings conducted in layer V of S1 and V1 while stimulating vM1. vM1 stimulation caused robust S1 activation concurrent with modest changes in V1. (B–D) Population data, comparing changes in S1 and V1 delta power (B), gamma power (C) and multiunit spiking (D). *, $p<0.05$.

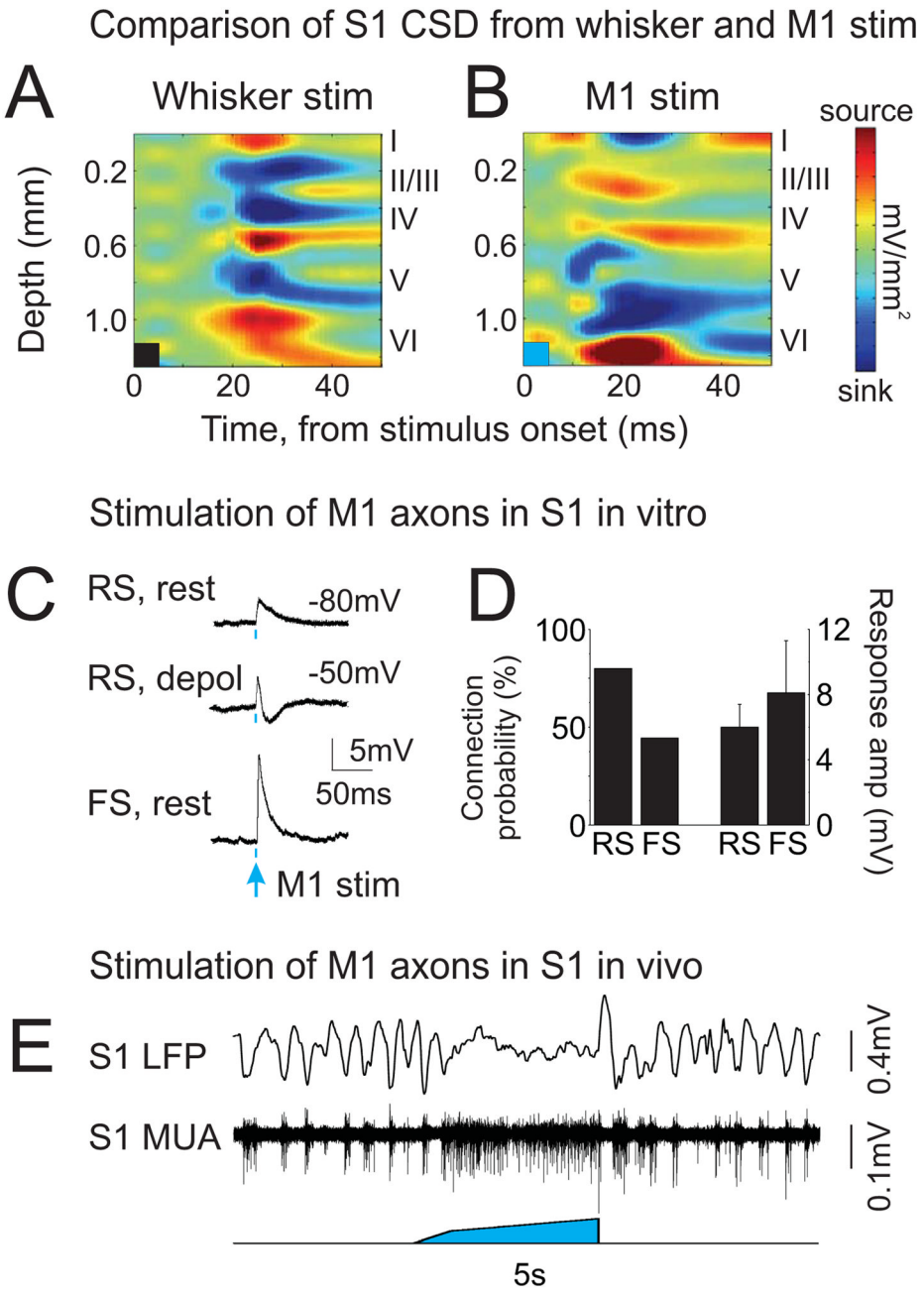

Figure 5. Evidence for involvement of the cortico-cortical feedback pathway

(A,B) CSD plots of average S1 responses from an example experiment. Brief (5 ms) deflections of the principal whisker (A) evoked onset current sinks in layers IV, II/III and V and current sources in layers I and VI. Brief (5 ms) vM1 stimuli (B) evoked onset current sinks in layers V, VI and layer I and current sources in layers II/III. Stimulus durations are depicted by the colored boxes in the bottom left of each plot. Color scales are +/−10 mV/mm^2 for whisker stimuli and +/−5 mV/mm^2 for vM1 stimuli. (C) Synaptic responses from layer V S1 neurons *in vitro*, evoked by stimulating axons and terminals of vM1 neurons in S1. The 2 ms light pulses are indicated by blue dots below traces. Responses from a regular spiking neuron (RS), consisting of a short latency EPSP at rest (top), and an EPSP-IPSP sequence (middle) when depolarized to just below spike threshold. Bottom, EPSP from a

fast spiking neuron (FS) at rest. (D) Population data, quantifying connection probabilities (left) and response amplitudes (right) from vM1 inputs onto regular spiking and fast spiking neurons in S1. (E) *In vivo* S1 response to stimulation of vM1 axons in S1. Limiting direct stimulation to the cortico-cortical vM1 axons was sufficient to evoke S1 activation. See also Supplemental Figure 3.

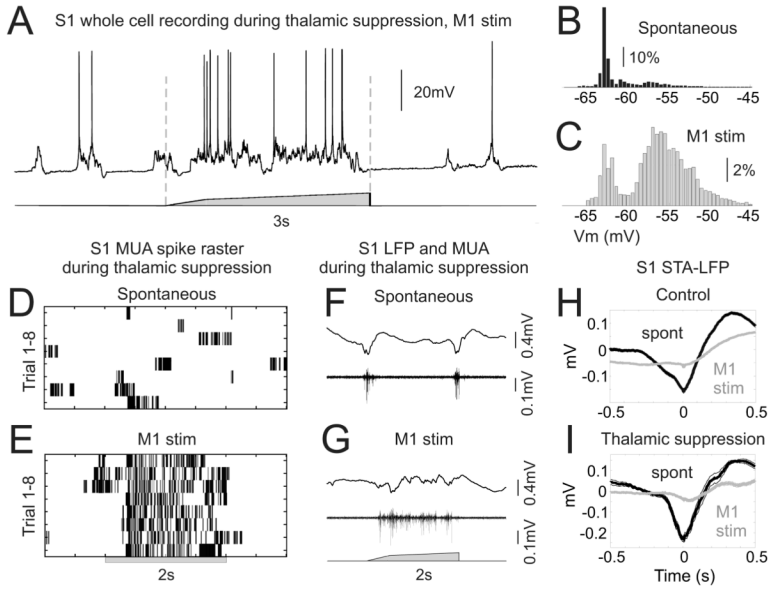

Figure 6. vM1 modulation of S1 activity does not require thalamocortical transmission

(A) A whole cell current clamp recording from a layer V S1 neuron, in response to a three second vM1 stimulus during thalamic suppression. Note the presence of prolonged hyperpolarized periods (Down states) in the spontaneous activity due to thalamic suppression, and the robust depolarization produced by vM1 stimulation. (B,C) Vm histograms of the neuron shown in [A], during spontaneous periods (B) and during vM1 stimulation (C). (D,E) S1 MUA spike rasters of spontaneous activity (D) and successive vM1 stimulation trials (E) during thalamic suppression. (F,G) Example data of S1 LFP (top) and MUA (bottom) during thalamic suppression for spontaneous activity (F) and in response to vM1 stimulation (G). (H,I) Spike-field relationships as calculated by the spike-triggered average of the LFP for spontaneous activity (black) and during vM1 stimulation (gray). Under both control (H) and thalamic suppression (I) conditions, vM1 stimulation abolished the phase-locking of spikes to the negative phase of the slow oscillation. See also Supplemental Figure 4.

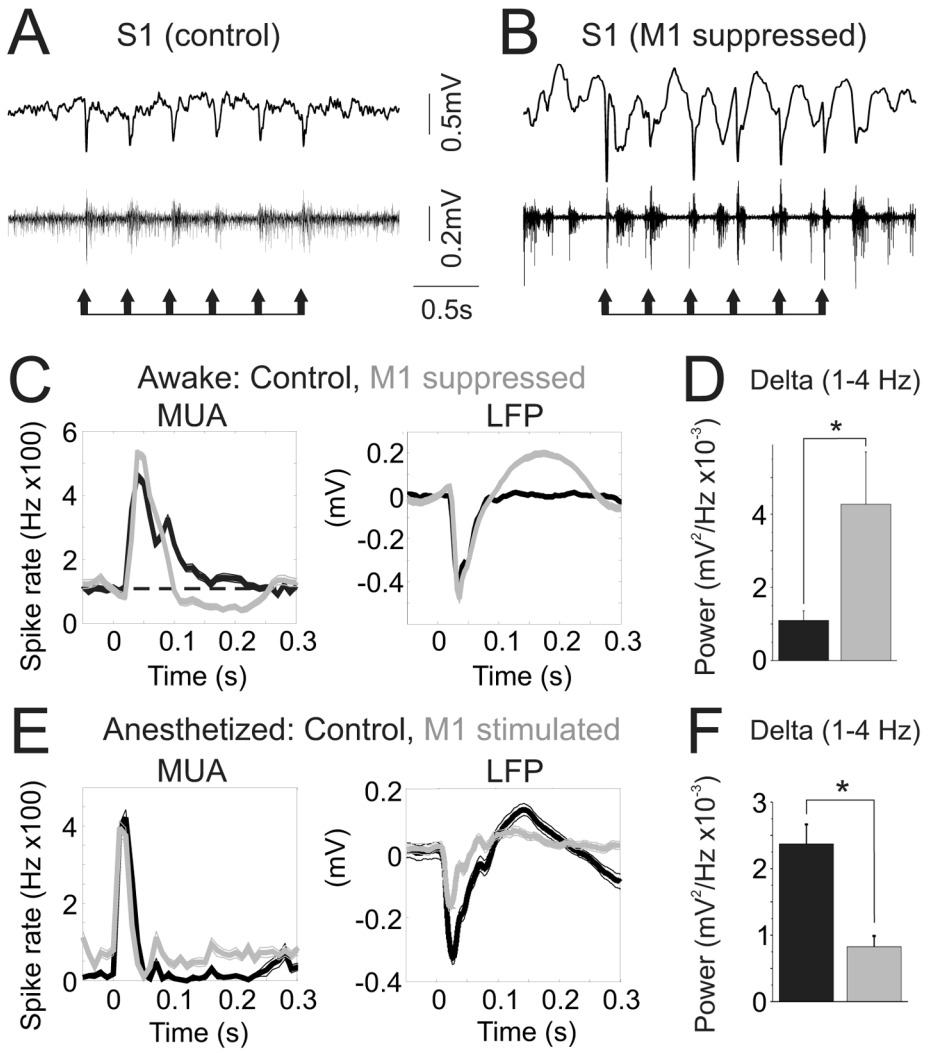

Figure 7. vM1 modulates S1 responses to simple sensory stimuli

(A,B) Single trial S1 LFP (top) and MUA (middle) responses to brief (10 ms) whisker stimuli in waking mice, before (A) and during (B) focal vM1 suppression. Stimuli are indicated by the arrows below the traces. (C) Average MUA (left) and LFP (right) responses to whisker stimuli for control (black) and vM1 suppression (gray) conditions from one experiment. The dashed line (C, left) indicates baseline firing rates. (D) Population data, S1 LFP delta power during sensory responses in control (black) and vM1 suppression (gray) conditions. (E–F) Experiments in anesthetized mice, pairing brief deflections of the principal whisker with vM1 stimulation. (E) Average MUA (left) and LFP (right) responses to whisker stimuli for control (black) and vM1 stimulation (gray) trials from one experiment. (F) Population data, S1 LFP delta power during sensory responses in control (black) and vM1 stimulation (gray) conditions. *, $p<0.05$.

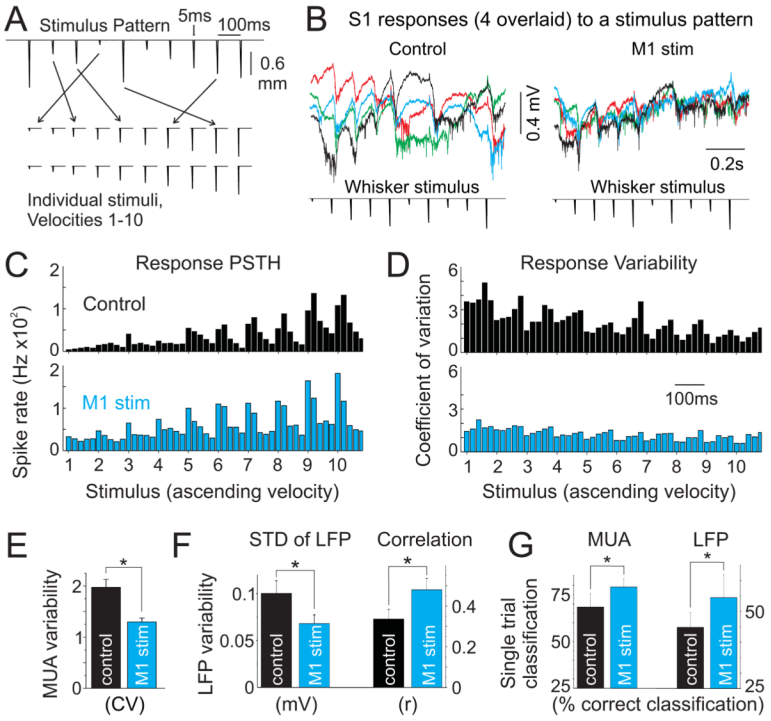

Figure 8. vM1 stimulation enhances S1 representation of complex stimuli

(A) Top, example stimulus pattern, consisting of 10 randomly ordered rapid deflections of the principal whisker delivered at 10 Hz. Bottom, resorting of stimulus patterns into individual stimuli according to velocity, which was used for CV analyses. (B) Single trial examples of raw data (0.3 Hz-5 kHz) from one experiment, showing four overlaid responses to the same whisker stimulus pattern (bottom) during control (left) and vM1 stimluation (right) conditions. (C) Multiunit spike histograms (20 msec bins) from the experiment in [B] in response to all whisker velocities, re-ordered from smallest [1] to largest [10] velocity, for control (black, top) and vM1 stimulation (blue, bottom) trials. Stimulus numbers along the x-axis are positioned at the onset of each whisker stimulus. (D) Corresponding CV for data shown in [C]. Note the reduced variability in MUA responses when paired with vM1 stimulation (bottom), particularly for smaller amplitude sensory stimuli. (E–G) Population data, comparing control (black) and vM1 stimulation (blue) trials. (E) MUA variability, calculated as the CV of MUA responses across all stimuli. (F) LFP variability, calculated as the mean standard deviation throughout the response period (left) and the mean correlation from pair-wise comparisons of individual trials (right). (G) Correct classification percentages from linear discriminant analyses of MUA (left) and LFP (right) stimulus pattern responses. Chance is 12.5% correct classification. *, $p<0.05$. See also Supplemental Figure 5.